

# Solvent Dependence of the Morphology of Spin-Coated Thin Films of Polydimethylsiloxane-Rich Polystyrene-*block*-Polydimethylsiloxane Copolymers

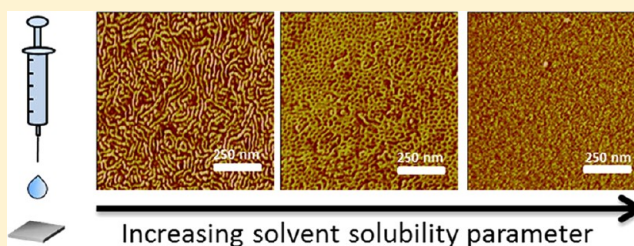
Maurice L. Wadley,<sup>†,§</sup> I-Fan Hsieh,<sup>‡</sup> Kevin A. Cavicchi,<sup>†,\*</sup> and Stephen Z. D. Cheng<sup>‡</sup>

<sup>†</sup>Department of Polymer Engineering, The University of Akron, Akron, Ohio 44325-0301, United States

<sup>‡</sup>Department of Polymer Science, The University of Akron, Akron, Ohio 44325-3909, United States

## S Supporting Information

**ABSTRACT:** The as-spun, thin film morphologies of a series polydimethylsiloxane-rich cylinder and lamellar-forming polystyrene-*block*-polydimethylsiloxane (PS-*b*-PDMS) copolymers with constant PDMS molecular weight and varying PS volume fraction were studied with a range of solvents of varying solubility parameter. It was found that PDMS occupies the surface of the thin films regardless of the choice of solvent used in spin-coating due to its extremely low surface tension. The morphology shifted from parallel cylinders to hexagonally perforated lamellar to parallel lamellar as the solvent was varied from PDMS to PS selective solvents (increasing solvent solubility parameter). The transition points between each morphology were also dependent on the volume fraction of the block copolymer where the transitions were observed at lower solubility parameter with increasing PS volume fraction of the polymer. The morphology variations are attributed to selective swelling effects of the individual blocks even under good solvent conditions. These results are discussed in the context of current theories of solvent evaporation induced ordering of block copolymer thin films.



## INTRODUCTION

Block copolymers are well-known to self-assemble into periodic, ordered nanostructures.<sup>1</sup> Typical length scales of microphase separation are on the order of 10–50 nm which provides an alternative for patterning surfaces compared to conventional lithographic techniques.<sup>2–4</sup> A variety of polymers have been studied ranging from thermoplastic elastomer based systems to photoresist analogues.<sup>5–7</sup> Block copolymers containing polydimethylsiloxane (PDMS) have recently attracted attention for patterning because of the conversion of PDMS into silicon oxide and the concurrent removal of the organic, non-PDMS block under ultraviolet/ozone or oxygen plasma treatment to produce topographically patterned silica in the forms of porous silica, perpendicular silica posts, parallel nanowires, and silica capsules.<sup>8–15</sup> In addition to this dry processing, these polymers also have a large interaction parameter useful for patterning low molecular weight polymers with high density nanostructures.<sup>16</sup>

The orientation of anisotropic morphologies is also important as perpendicular orientations of cylinders and lamellar with respect to the substrate are desirable for high aspect ratio nanostructures for surface patterning.<sup>17,18</sup> Many different cylinder-forming block copolymers, including PDMS-rich and PDMS-poor, are oriented perpendicularly during solvent casting by judicious choice of the solvent.<sup>19–24</sup> One proposed mechanism for evaporation induced orientation is that the ordering of the polymer at the free surface forms a seed

layer of perpendicular cylinders, which propagates into the film due to a gradient in the solvent concentration during evaporation and are then kinetically trapped by the vitrification of one of the blocks.<sup>21,25,26</sup> It is known that solvents can shift the relative concentrations of the blocks at the surface due to their selectivity.<sup>18</sup> Therefore, it has been suggested that choosing a solvent that has a higher affinity for the block with the larger surface tension mediates the interactions to produce the perpendicular cylinder seed layer during casting.<sup>27</sup> However, the recent example of perpendicularly oriented cylinders from PDMS-rich polystyrene-*block*-PDMS (PS-*b*-PDMS) copolymer is an exception to this rule as the polymer was cast from dodecane, which is a selective for PDMS based on the larger solubility parameter differences of PS (18.6 MPa<sup>1/2</sup>) and dodecane (16.0 MPa<sup>1/2</sup>) compared to PDMS (15.2 MPa<sup>1/2</sup>) and dodecane.<sup>13,28,29</sup>

This article describes the investigation of the as-spun thin film morphology of a series of low molecular weight PDMS-rich PS-*b*-PDMS copolymers ( $0.54 \leq f_{\text{PDMS}} \leq 0.72$ ) from a range of different solvents over a range of solubility parameters. It is shown that PDMS-rich surfaces are obtained regardless of solvent choice. This is attributed to the surface activity of the low surface tension PDMS block. In addition, a range of surface

Received: January 6, 2012

Revised: May 14, 2012

Published: June 22, 2012

morphologies are observed depending on the casting solvent and the volume fraction of the polymer. These results are interpreted as being driven by the selective swelling of either the PDMS or PS block shifting the as-cast morphology during evaporation induced ordering. These results are contrasted with those previously reported for another PDMS-rich PS-*b*-PDMS polymer system where perpendicularly oriented cylinder morphologies were obtained.<sup>13</sup> With the aid of a recent model for the evaporation driven orientation of block copolymer guidelines are proposed for controlling the thin film orientation of PDMS-rich block copolymers.<sup>30</sup>

## EXPERIMENTAL SECTION

**Materials.** Asymmetric PS-*b*-PDMS copolymers were synthesized by reversible addition–fragmentation chain transfer (RAFT) polymerization by a previously reported method in which the styrene monomer was polymerized in the presence of a 10 kg mol<sup>−1</sup> PDMS macro RAFT agent.<sup>31</sup> Four polymers were synthesized with this technique with increasing PS volume fractions,  $f_{\text{PS}}$ , of 0.28, 0.32, 0.39, and 0.46. Solvents used for preparing thin films were purchased from VWR and used as received.

**Sample Preparation and Characterization.** Polymer solutions (10 mg/mL) were spun-coat at 3000 rpm on PDMS-brush coated silicon substrates. Spin-coating was performed using a Laurell Technologies WS-400B-6NPP/Lite spin-coater at room temperature. The spin-coater chamber was under a constant purge of nitrogen during use. Silicon wafer substrates ((100)-oriented, n-type/phosphorus doped) were purchased from Silicon Quest International. The native oxide layer of the Si wafer was modified with a PDMS brush layer by spin-coating a thin film from a 10 wt % toluene solution of hydroxy-terminated PDMS homopolymer (molecular weight: 10 kg mol<sup>−1</sup>, Gelest, USA), which was annealed under vacuum at 180 °C for 24 h to end-tether the PDMS to the wafer surface. The unattached polymer was washed off with toluene. Scanning force microscopy (SFM) measurements were performed in an ambient environment with a multimode Veeco Nanoscope IIIa in tapping mode. SFM tips used were model RTESPW from Veeco. Static water contact angle measurements were carried out using a Ramé-Hart model 500 advanced goniometer with DROPImage Advanced v.2.4 software. A droplet of deionized water was deposited onto the surface and images were captured by video camera after 1 min. Image analysis by the software determined the contact angle from the shape of the droplet. Reported contact angles are an average of seven measurements per sample. Film thickness was measured using a Filmetrics F20 interferometer. Small-angle X-ray scattering (SAXS) experiments were performed using a Rigaku SAXS and wide-angle X-ray scattering (WAXD) instrument with an 18 kW rotating anode X-ray generator (MicroMax-002<sup>+</sup>) equipped with a Cu tube operated at 45 kV and 0.88 mA. The wavelength of the X-ray beam was 0.15418 nm. The zero pixel of the SAXS patterns was calibrated using silver behenate with the first-order scattering vector,  $q$ , being 1.076 nm<sup>−1</sup> ( $q = 4\pi(\sin \theta)/\lambda$ , where  $\lambda$  is the wavelength and  $2\theta$  is the scattering angle). SAXS samples were dissolved in toluene and cast at room temperature. Samples were then put into the vacuum oven at 100 °C for 4 days, and then annealed at 150 °C for an additional 2 days. SAXS data was collected at room temperature. For transmission electron microscopy (TEM) characterization a solution of 10 mg/mL PS-*b*-PDMS in ethyl acetate was spin-coated on carbon-coated mica with a spin rate of 3000 rpm for 60 s. Before spin coating, ethyl acetate was spin coated on the carbon-coated mica to increase the wetting ability of the sample solution. After spin coating, the thin film sample was removed from the substrate by immersing the thin film sample into a water bath and picked up with a TEM copper grid. The morphology of PS-*b*-PDMS thin film was examined by TEM (JEOL JEM-1230) operated at 120 kV in bright field.

## RESULTS AND DISCUSSION

**1. Bulk Morphology.** A series of PS-*b*-PDMS copolymers spanning a range of polystyrene volume fractions,  $f_{\text{PS}}$ , of 0.28–0.46 were prepared using a PDMS macro-RAFT agent. The molecular weight characteristics of the polymers are given in Table 1.<sup>32</sup> The bulk morphologies of the four PS-*b*-PDMS

**Table 1.** PS-*b*-PDMS Copolymer Characteristics

sample ID	$f_{\text{PS}}^a$	$M_{\text{PS}}^a$ (g/mol)	$M_{\text{PDMS}}^b$ (g/mol)	PDI <sup>c</sup>
PS- <i>b</i> -PDMS 4.2–10	0.28	4200	10 000	1.08
PS- <i>b</i> -PDMS 5.2–10	0.32	5200	10 000	1.09
PS- <i>b</i> -PDMS 6.9–10	0.39	6900	10 000	1.09
PS- <i>b</i> -PDMS 9.4–10	0.46	9400	10 000	1.09

<sup>a</sup>Calculated from <sup>1</sup>H NMR spectra using  $\rho_{\text{PDMS}} = 0.97 \text{ g/cm}^3$  and  $\rho_{\text{PS}} = 1.05 \text{ g/cm}^3$ . <sup>b</sup>Reported by the manufacturer. <sup>c</sup>From SEC analysis calibrated with PS standards.

copolymers were determined using SAXS and are shown in Figure 1. For the PS-*b*-PDMS 4.2–10 and PS-*b*-PDMS 5.2–10

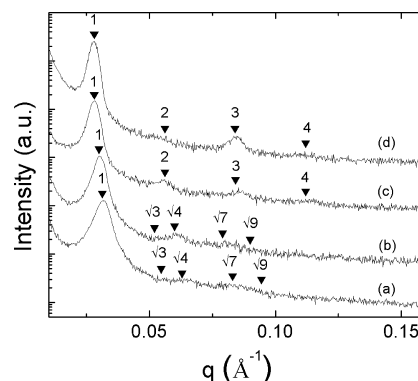


**Figure 1.** Azimuthally averaged 1D SAXS profiles of bulk PS-*b*-PDMS copolymers (a) PS-*b*-PDMS 4.2–10 (b) PS-*b*-PDMS 5.2–10 (c) PS-*b*-PDMS 6.9–10 (d) PS-*b*-PDMS 9.4–10 at ambient conditions. The expected  $q/q^*$  positions are shown for cylinders (a, b) and lamellar (c, d).

polymers peak sequences consistent with a cylinder morphology were observed ( $1:\sqrt{3}:\sqrt{4}:\sqrt{7}:\sqrt{9} \ q/q^*$ ). The first-order scattering peaks of the PS-*b*-PDMS 4.2–10 and PS-*b*-PDMS 5.2–10 copolymers correspond to a  $d_{100}$  plane spacing ( $2\pi/q^*$ ) of 19.9 and 20.9 nm with cylinder diameters of 12.8 and 14.4 nm, respectively, calculated from the relative volume fractions and geometry of the hexagonal lattice. Form factor minima calculated at  $q^* \approx \sqrt{3}$  for the cylinder forming copolymers explain the attenuated  $q/q^* = \sqrt{3}$  peak of both polymers.<sup>33</sup> For the PS-*b*-PDMS 6.9–10 and PS-*b*-PDMS 9.4–10 copolymers a Bragg scattering peak sequence of  $1:2:3:4 \ q/q^*$  was expected for a lamellar morphology. For PS-*b*-PDMS 6.9–10 copolymer there was no overlap of the calculated form factor minima while for PS-*b*-PDMS 9.4–10 copolymer form factor minima were calculated to overlap at both  $q^* = 2$  and 4 explaining the absence of those peaks.<sup>33</sup> The first-order scattering peaks corresponded to a domain spacing of 22.4 nm for both lamellar-forming copolymers. One possible reason for the identical domain spacing in the two polymers is as follows. It has been observed that the PS-*b*-PDMS phase diagram is skewed, with the phase boundaries shifted toward low PS volume fractions.<sup>34</sup> Theoretical calculations by Matsen and



Bates have shown that in a phase diagram of this type the domain spacing relative to the radius of gyration of the polymer actually decreases with increasing PS volume fraction in the lamellar region at  $f_{\text{PS}} < 0.5$ , contrary to what is expected for a symmetric phase diagram.<sup>35</sup> Therefore, the increase in the  $R_g$  due to the larger PS block could be balanced by the decreased stretching resulting in the same domain spacing in the two polymers.

**2. PS-*b*-PDMS Thin Film Morphology.** Thin films were prepared with each copolymer by spin-coating using a range of solvents (in order of total Hansen solubility parameter,  $\delta$ , in  $\text{MPa}^{1/2}$ : *n*-hexane (14.7), *n*-heptane (15.3), methylcyclohexane (16.0), cyclohexane (16.7), butyl acetate (17.4), *n*-propyl acetate (17.6), ethyl acetate (18.5), benzene (18.6), methyl ethyl ketone (19.1), chlorobenzene (19.5), cyclohexanone (19.6), and 1,4-dioxane (20.5)).<sup>28</sup> Homogeneous, transparent solutions were obtained at 1 wt % copolymer concentration for each copolymer–solvent combination. This is a typical concentration used for the preparation of thin films on the order of tens of nanometers thick.<sup>12,13,15</sup> It was found that uniform films were always generated on the PDMS brush coated wafers compared to bare silicon wafers. In the latter case, poor film coverage was obtained intermittently. As the source of this phenomenon could not be ascertained, all experiments used PDMS treated wafers. Figure 2 shows SFM phase images of five representative surface morphologies obtained from spin-coated films. In these phase images the stiffer PS domains appear brighter than the softer PDMS domains. With increasing solubility parameter the thin film surface morphologies shift from bright lines (Figure 2a), to a mixture of spots and lines (Figure 2b), to an array of predominately dark spots (Figure 2c), to sparsely populated dark spots (Figure 2d), to a predominately featureless surfaces (Figure 2e). Figure 2 shows a clear dependence of the solvent choice on the surface morphology of the as-cast films. The full set of SFM phase images and the as-spun film thicknesses are given in the Supporting Information (Table S1, Figure S3). In some of the films, especially in higher solubility parameter solvents larger scale terracing of the films is observed. Therefore, the measured film thickness likely represents an average film thickness in these cases. In Figure 3, the surface morphology is plotted as a function of the solubility parameter of the spin-coating solvent and  $f_{\text{PS}}$  of the four PS-*b*-PDMS copolymers. While in higher solubility parameter solvents the images consisted of predominately featureless regions, in most cases there were still sparsely distributed dark spots and or lines and were categorized as sparsely populated dark spots. For PS-*b*-PDMS 9.4–10 in cyclohexanone and 1,4-dioxane it was difficult to categorize the morphology as good SFM images were difficult to obtain without significant drift and are therefore omitted from Figure 3. This morphology diagram shows that for each PS-*b*-PDMS copolymer a similar sequence of surface morphologies is observed with increasing solubility parameter of the casting solvent. The transition points in this sequence shift to lower solvent solubility parameter as the  $f_{\text{PS}}$  in the polymers increases. This transition sequence was found to be most dependent on the solubility parameter of the casting solvent. For example, qualitatively identical surface morphologies were obtained when solvents with different vapor pressures, but similar solubility parameters were used in Figure 4. To confirm that these surface morphologies were a result of the spin-coating process, the films spun-coat from cyclohexane ( $\delta = 16.7 \text{ MPa}^{1/2}$ ) and *n*-propyl acetate ( $\delta = 17.6 \text{ MPa}^{1/2}$ ) were

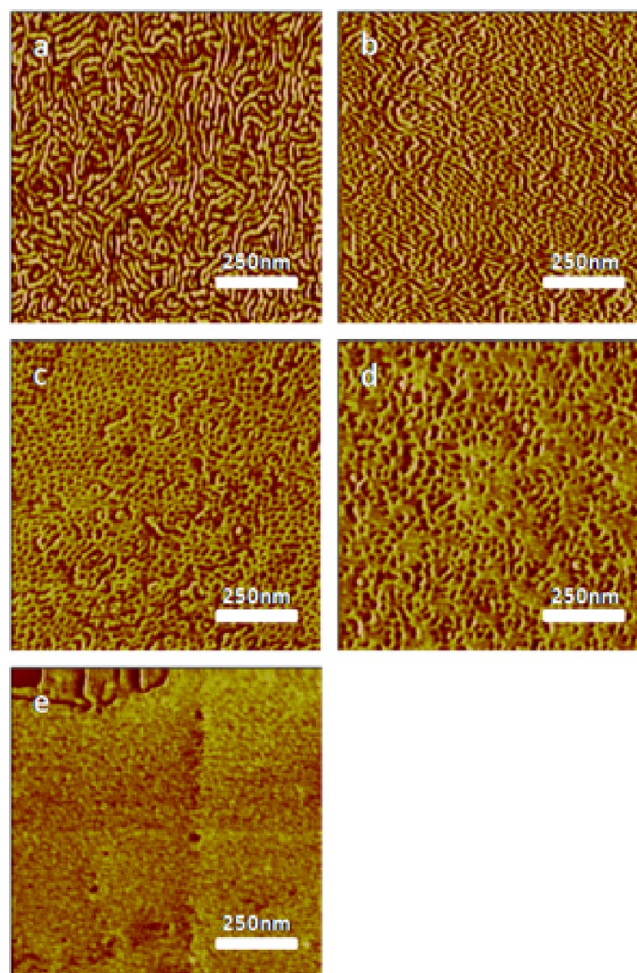


**Figure 2.** Representative SFM phase images of as spun PS-*b*-PDMS 4.2–10 on 10k  $M_w$  PDMS–OH treated wafer spin-coated at 10 mg/mL in order of increasing Hansen solubility parameter: (a) *n*-hexane, (b) butyl acetate, (c) ethyl acetate, (d) methyl ethyl ketone, and (e) cyclohexanone.

thermally annealed overnight under vacuum at 180 °C. Figure 5 shows the SFM phase images of the thermally annealed copolymer samples for each volume fraction. For each copolymer, even though the as-spun morphologies were different, identical morphologies are obtained after annealing. This is further demonstrated in Figure 6 where the thermally annealed surface morphology is predominately invariant with the solubility parameter of the casting solvent for each PS volume fraction after thermal annealing. Some anomalies were observed in the PS-*b*-PDMS 5.2–10 copolymer thin films cast from butyl acetate, chlorobenzene, cyclohexanone, and 1,4-dioxane. This may be influenced by a synergistic effect of low film thickness (<25 nm), and solvent volatility.<sup>36</sup> In thinner films confinement effects could also influence the film morphology, which depend on the interfacial energies of the air and substrate interface and the polymer volume fraction.<sup>22</sup> From the SAXS characterization of the bulk morphology in Figure 1, the expected morphology of the PS-*b*-PDMS 4.2–10 and PS-*b*-PDMS 5.2–10 polymers is parallel cylinders and for PS-*b*-PDMS 6.9–10 and PS-*b*-PDMS 9.4–10 the expected morphology is parallel lamellar. Therefore, the line and featureless morphologies of Figure 3 and Figure 5 are assigned as parallel cylinders ( $\parallel$  C) and parallel lamellar ( $\parallel$  L)



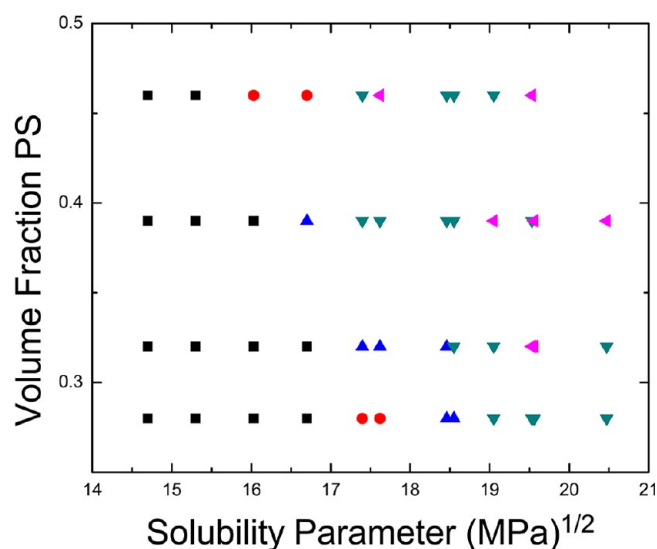


**Figure 3.** Surface morphology of as cast films for PS-*b*-PDMS copolymer thin films with increasing PS volume fraction plotted vs Hansen solubility parameter of the casting solvent. The patterns observed include: bright lines (black square), bright lines + dark spots (red dot), dark spots (blue triangle), sparsely populated dark spots (green triangle), and predominately featureless (pink triangle).

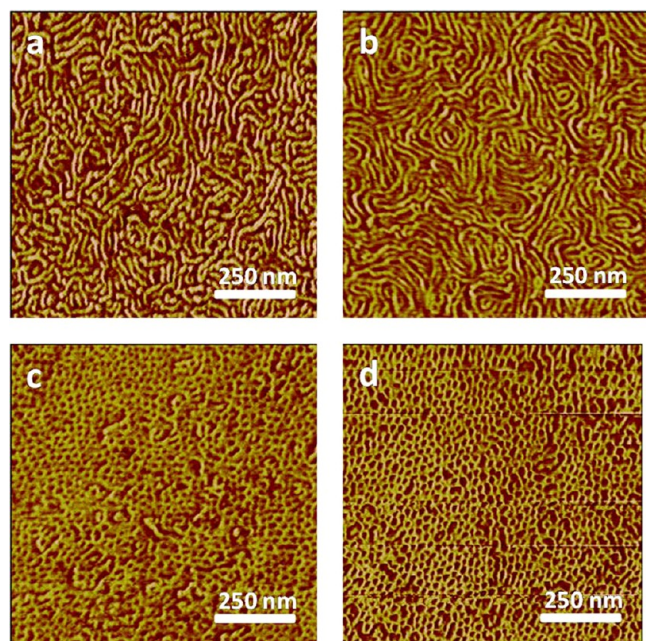


**Figure 4.** As-cast surface morphology of PS-*b*-PDMS 4.2–10 copolymer films spin-coated from (a) *n*-hexane ( $\delta = 14.7$ , vapor pressure = 128 mmHg at 21 °C) (b) diethyl ether ( $\delta = 14.7$  MPa<sup>1/2</sup>, vapor pressure = 462 mmHg at 21 °C) (c) ethyl acetate ( $\delta = 18.5$  MPa<sup>1/2</sup>, vapor pressure = 78 mmHg at 21 °C), and (d) chloroform ( $\delta = 19.0$  MPa<sup>1/2</sup>, vapor pressure = 169 mmHg at 21 °C) at 10 mg/mL concentration.<sup>28</sup>

respectively. The other main surface morphology observed was dark spots. It is known that hexagonally perforated lamellar (HPL) morphologies can be stabilized in thin films.<sup>12,22,23,37–43</sup> This is consistent with the spot patterns where a PS lamellar layer is perforated by hexagonally packed PDMS domains. It should be noted that perpendicular cylinders of PS in PDMS would be expected to appear as bright dots in a dark matrix due

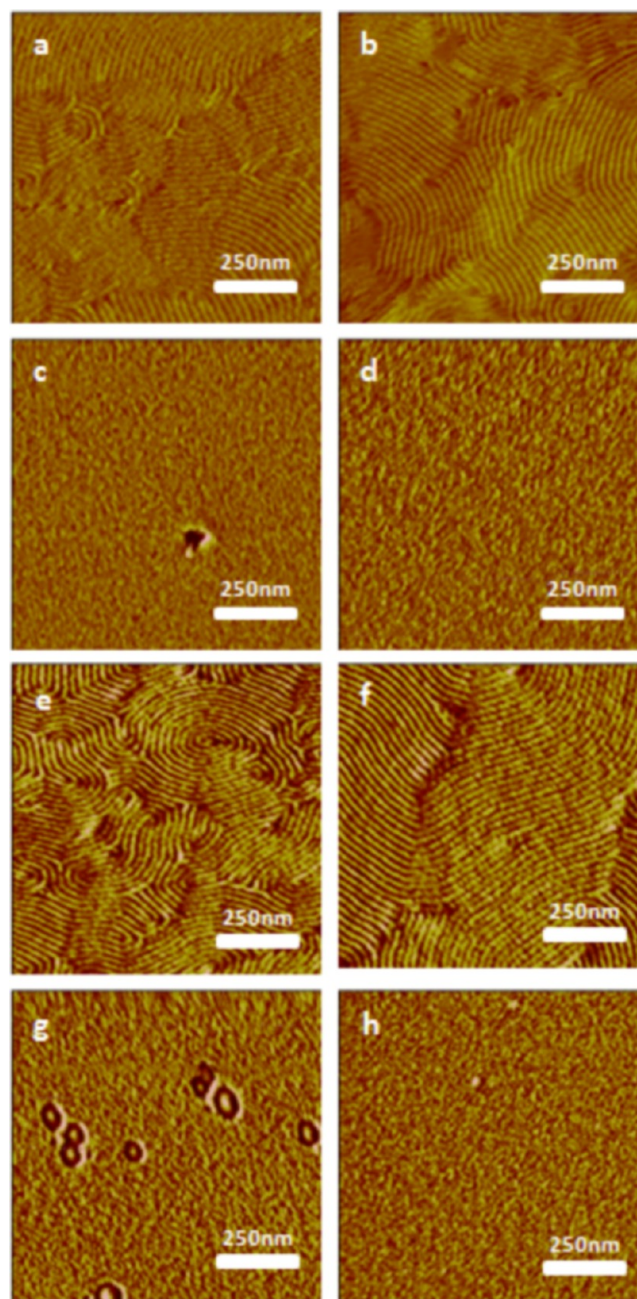


**Figure 5.** Thermally annealed thin film morphology spin-coated in *n*-propyl acetate, (a) PS-*b*-PDMS 4.2–10, (b) PS-*b*-PDMS 5.2–10, (c) PS-*b*-PDMS 6.9–10, and (d) PS-*b*-PDMS 9.4–10, and in cyclohexane, (e) PS-*b*-PDMS 4.2–10, (f) PS-*b*-PDMS 5.2–10, (g) PS-*b*-PDMS 6.9–10, and (h) PS-*b*-PDMS 9.4–10.

to the higher stiffness of the PS block in the phase image. HPL surface morphologies are usually seen in between regions where parallel cylinder and lamellar surface morphologies are stabilized.<sup>22,23,44</sup> In the bulk, the HPL phase is metastable between the cylinder and lamellar regions where the gyroid phase is thermodynamically more favorable.<sup>45</sup> But, the HPL phase has been observed as a transient morphology on the ordering transition between cylinders and lamellae.<sup>46</sup> The lower stability of the HPL morphology is also apparent as both cylinder-HPL (Figure 2b) and HPL-lamellar (Figure 2d) are observed. A sample for transmission electron microscopy (TEM) was also prepared by spin-coating a 10 mg/mL solution

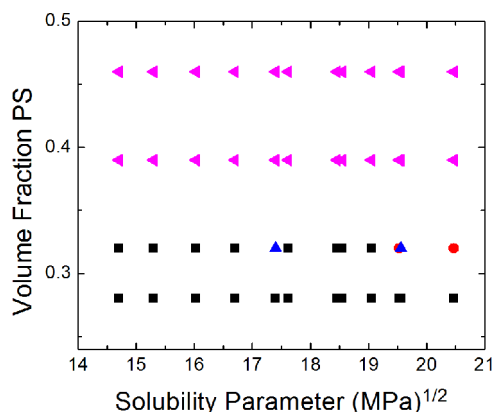


**Figure 6.** Surface morphology of thermally annealed PS-*b*-PDMS copolymer films at 180 °C for 24 h. The observed morphologies include bright lines (black square), bright lines + dark spots (red dot), dark spots (blue triangle), and featureless regions (pink triangle).

of PS-*b*-PDMS 4.2–10 in ethyl acetate onto a carbon coated mica substrate and then transferred to a TEM grid. The sample dewet the substrate during spin-coating, therefore it could be imaged in very thin regions. The TEM micrograph is shown in Figure S2 in the Supporting Information. The PDMS appears darker due to the higher electron density. In the thinner region in the upper right-hand corner of the micrograph round domains of PDMS surrounded by PS consistent with HPL are observed. A transition to parallel cylinders occurs as the film thickness increases toward the lower left-hand corner. This sequence from HPL to cylinders with increasing thickness is consistent with what has previously been observed in dewetted films.<sup>44</sup> In the thicker film, the morphology is more difficult to discern likely due to overlaying multiple layers. The surface morphology is clearer in the SFM characterization as it only is sensitive to the film surface. Therefore, it is also unknown how far these morphologies propagate into the films.

**3. PS-*b*-PDMS Thin Film Surface Activity.** To further characterize the surface morphology the water contact angle of the as-spun and thermally annealed films was measured. The water contact angles of PDMS and PS have been reported as ranging from 105 to 112° and from 86 to 90°, respectively.<sup>47–50</sup> The as spun films and the thermally annealed films were found to have water contact angle ranges of 103–116° and 104–107°, respectively, indicating that all of the films made were PDMS-rich regardless of solvent choice for spin-coating. The contact angles for the as-spun films are provided in the Supporting Information (Figure S1, Table S1). This result of PDMS-rich surfaces has been generally observed in PS-*b*-PDMS films.<sup>9,29,50–52</sup> For example, Clark et al. studied the surface compositions of PS-*b*-PDMS copolymer films with 23 and 59 wt % PS using X-ray photoelectron spectroscopy and found that there existed a pure PDMS layer ranging from 1.3–4 nm thick at the surface regardless of casting solvent.<sup>53</sup> An explanation for this behavior is obtained by considering the relative surface tensions of the blocks. The surface tension of PDMS ( $\gamma = 19.9$  mN/m) is dramatically lower than that of PS ( $\gamma = 40.7$  mN/m) which drives the PDMS toward the surface in PDMS selective solvents and during thermal annealing.<sup>54</sup> The low surface tension of PDMS also raises the possibility that it is surface active in the higher surface tension solvents. For example the surface tension of PDMS is lower than that of all of the solvents used in this study except hexane and *n*-heptane as shown in Table 2. This is fairly unique as PDMS has one of the

**Table 2.** Solubility Parameter, Surface Tension, and  $S_{\text{PDMS}}$  for Each Solvent

solvent	$\delta$ (MPa) <sup>1/2</sup>	surface tension $\gamma$ (mN/m)	$S_{\text{PDMS}}$
hexane	14.7	17.9	−2.5
<i>n</i> -heptane	15.3	19.7	−0.4
methylcyclohexane	16.0	23.3	2.6
cyclohexane	16.7	24.7	3.5
<i>n</i> -butyl acetate	17.4	24.9	3.3
<i>n</i> -propyl acetate	17.6	23.8	2.1
ethyl acetate	18.5	23.4	1.2
benzene	18.6	28.2	6.0
methyl ethyl ketone	19.1	24.0	1.5
chlorobenzene	19.5	33.0	10.2
cyclohexanone	19.6	34.6	11.8
1,4-dioxane	20.5	32.8	9.5

lowest surface tensions for polymers, besides fluoropolymers. In fact, PS-*b*-PDMS has been shown to be surface active in benzene, ethyl benzoate, bromoethyl benzoate, and dioctyl phthalate.<sup>55–57</sup> The condition for surface activity is that the spreading parameter,  $S$ , is positive, where  $S$  is given by<sup>58</sup>

$$S = \gamma_{\text{air/solvent}} - \gamma_{\text{air/polymer}} - \gamma_{\text{polymer/solvent}} \quad (1)$$

where  $\gamma_{\text{A/B}}$  is the interfacial tension between components A and B. The air/polymer and air/solvent surface tensions are tabulated in various handbooks.<sup>29,54,59,60</sup> To estimate the surface tension between the polymer and solvent the following generalized empirical relationship was used<sup>61</sup>

$$\gamma_{\text{polymer/solvent}} = 0.881[\Sigma(\Delta\delta_i)^2]^{0.402} \quad (2)$$

where  $\Delta\delta_i$  is the difference in the dispersion ( $\delta_d$ ), dipolar ( $\delta_p$ ), and h-bonding ( $\delta_h$ ) components of the total solubility parameter. Here the total Hansen solubility parameter,  $\delta_t$ , was used due to the lack of values for component parameters for PDMS in the literature. The surface tension at 25 °C and the calculated  $S_{\text{PDMS}}$  are tabulated in Table 2 for each solvent. For every solvent except hexane and *n*-heptane,  $S_{\text{PDMS}}$  is positive, indicating that PDMS will wet the surface. This explains why PDMS enriches the film surface regardless of the casting solvent. The PDMS block likely migrates to the droplet surface in the spin-coater and then templates a parallel oriented morphology. Therefore, it would be difficult to obtain neutral surface conditions in PDMS-containing polymers through the solvent choice during solvent casting. However, one possible option to counteract the PDMS surface activity is to use environmental spin-coating.<sup>62</sup> Given the SFM and contact angle results a schematic of the different surface morphologies is shown in Figure 7. The trend of the surface morphology is not dependent on the spreading parameter and instead depends more strongly on the solubility parameter of the solvent. This

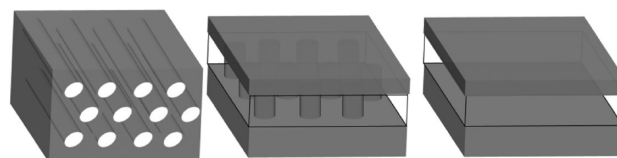


**Figure 7.** Schematic of the surface morphologies observed from PS-*b*-PDMS thin films. The PDMS domains are depicted in gray, while the PS domains occupy the open areas. From left to right: parallel cylinders, hexagonally perforated lamellar, and lamellar.



implies that the morphology depends on the interactions between the blocks and the casting solvent and is the subject of the next section.

**4. PS-*b*-PDMS Surface Morphology.** The next question to answer is: why does the surface morphology depend on the casting solvent? In this case the morphology is not strongly dependent on the spreading parameter, but tracks more closely with the solubility parameter. One possibility is that as the solvent becomes more favorable for one block it selectively swells those chains shifting the spontaneous curvature of the morphology during evaporation induced ordering. As the film is cast the equilibrium morphology is changing with solvent concentration, which could result in order–order transitions during casting. At the same time the chain dynamics are also rapidly slowing down during solvent evaporation leading to vitrification of the PS domains and kinetic trapping of the film morphology. The morphology vs concentration dependence varies with the solvent selectivity and the asymmetry of the polymer leading to different kinetically trapped morphologies. In the case where order–order transitions occur during casting a mixed morphology could occur due to the fast evaporation as seen in Figure 3.

The interaction parameter for a polymer–solvent pair can be estimated from the solubility parameters of the polymer and solvent as

$$\chi_{12} = [V_m(\delta_1 - \delta_2)^2]/RT \quad (3)$$

where  $V_m$  is the molar volume of the solvent.  $\chi_{PS}$  and  $\chi_{PDMS}$  at 298 K are plotted as a function of the solubility parameter in Figure 8 and the polynomial fits to the curves intersect at  $\delta =$

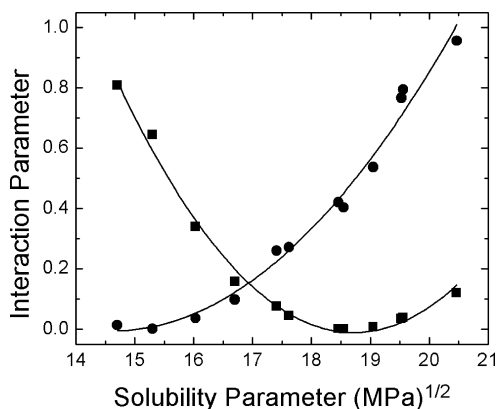


**Figure 8.** Calculated solvent-polymer interactions parameters for PS (■) and PDMS (●) as a function of solvent solubility parameter.

16.9 MPa<sup>1/2</sup>. This intersection is an estimate of the neutral solvent condition. The neutral solvent prediction in Figure 8 can be compared with the results of Figure 3. Near  $\delta = 16.9$  MPa<sup>1/2</sup> the thin film surface morphology is representative of the bulk morphology. For the cylinder forming samples (PS-*b*-PDMS 4.2–10 and PS-*b*-PDMS 5.2–10) increasing the solvent selectivity toward the PS block results in a shift of the morphology from || C → HPL → || L. The effect of the volume fraction is seen where the transitions from || C → HPL → || L occur at higher  $\delta_{\text{solvent}}$  in the lower  $f_{PS}$  block copolymers. This reflects that a higher solvent selectivity or preferential swelling is needed to shift the spontaneous curvature to obtain a new morphology. Similar results are seen in the lamellar forming samples (PS-*b*-PDMS 6.9–10 and PS-*b*-PDMS 9.4–10) where

the morphological transitions are observed in increasingly PDMS selective solvents. Below  $\delta = 15.5$  MPa<sup>1/2</sup> the solvents should be strongly selective for PDMS as  $\chi_{PS-\text{solvent}} > 0.5$  indicating poor solvent conditions at high PS molecular weight.<sup>63</sup> Similar conditions are obtained as  $\delta > 19$  MPa<sup>1/2</sup> where the solvents are strongly selective toward PS. Selective solvents are known to drive order–order transitions.<sup>64</sup> Transitions of a cylinder forming block copolymer to a perforated lamellar thin film structure were recently observed in a PS-*b*-PDMS system using mixed solvent vapors of slightly selective and highly selective solvents.<sup>12</sup> A similar shift from cylinders to HPL and lamellar to HPL was observed in poly(ethylene oxide) (PEO) based triblock copolymers by changing the relative humidity where water is highly selective toward the PEO block.<sup>65</sup> A recent study on the morphology of a cylinder forming poly( $\alpha$ -methylstyrene)-*block*-poly(4-hydroxystyrene) annealed in nonselective and selective solvents showed a reversible morphology between spheres and cylinders.<sup>66</sup> What is notable in the PS-*b*-PDMS thin films studied here is the shift of the surface morphology occurs under good solvent conditions for both blocks where selective swelling should be less prominent.<sup>67</sup>

A range of different ordered phases have been observed in polystyrene-*block*-polybutadiene, polystyrene-*block*-polybutadiene-*block*-polystyrene, and polystyrene-*block*-poly(methyl methacrylate) copolymers in slightly selective solvents by quenching and freeze-drying slowly evaporating solutions at different times to capture the film morphology at different solvent concentrations.<sup>41,68–71</sup> With cylinder-forming block copolymers a range of phases are seen moving toward the equilibrium morphology including inverted phases such as spheres, cylinders, and HPL where the minority block formed the matrix in these morphologies. In these PS-*b*-PDMS copolymer films, the fast evaporation conditions of spin coating appears to allow for the vitrification of the nonequilibrium cylinder, HPL, and lamellar morphologies. An interesting question for further study is whether the HPL morphology that is kinetically trapped during spin-coating is an equilibrium morphology in the solvent swollen state analogous to the observation of HPL in solvent annealed PS-*b*-PDMS thin films or an intermediate morphology trapped during an ordering transition from lamellar to cylinders.<sup>12,31</sup> The second explanation of an intermediate morphology could also explain the high coexistence of cylinders and lamellar with HPL during spin-coating.

The surface activity of the PDMS in these polymers offers an explanation for why the solvent was not able to mediate the interactions toward neutral conditions favorable for perpendicular domain orientation with PS selective solvents and instead resulted in a range of parallel morphologies. It is instructive to compare these results to Chao et al. who did observe perpendicular cylinders when casting a PS-*b*-PDMS 12–22 copolymer from dodecane ( $\delta = 16.0$  MPa<sup>1/2</sup>).<sup>13,28</sup> This solvent has a solubility parameter close to methylcyclohexane and is therefore a good solvent for PDMS and PS, but has a stronger affinity for PDMS. The polymer studied has a similar  $f_{PS}$  to PS-*b*-PDMS 5.2–10, which forms parallel cylinders when cast from solvents with  $\delta < 17$  MPa<sup>1/2</sup>. A recent model by Phillip et al. indicates that one key factor in evaporation induced orientation is the relative growth rate of the cylindrical domains in the drying film as a function of solvent concentration profile in the film.<sup>30</sup> If the growth rate is faster with increasing solvent concentration then a perpendicular cylinder orientation will

form due to the solvent gradient from the surface of the drying film. This growth rate depends on the competition between the thermodynamic driving force for ordering, which increases with decreasing solvent concentration versus the kinetic driving force for ordering, which decreases with decreasing solvent concentration. The authors also comment that the evaporation rate in the film is crucial for determining the orientation, where slow evaporation rates are less likely to generate a large enough concentration gradient to favor conditions for perpendicular cylinder growth. While forming a seed layer of perpendicular cylinders under neutral surface conditions is one method to initiate perpendicular cylinder growth, Phillip et al. hypothesize an alternative mechanism using selective solvent conditions for the matrix forming block driving sequential order–order transitions from disorder to spheres to cylinders.<sup>30,72</sup> Perpendicular ordering then occurs by the epitaxial growth of cylinders from spheres with the evaporation front.<sup>35</sup> An example of this mechanism is the use of mixed solvents when casting polystyrene-*block*-polyvinylpyridine copolymer to drive a transition from micelles to cylinders resulting in a perpendicular cylinder orientation.<sup>73</sup> According to the model by Phillip et al., this condition is met when the solvent concentration in the film ( $\phi_s$ ) is less than the critical solvent concentration for perpendicular ordering ( $\phi_{sc}$ ) given by

$$\phi_{sc} = \phi_{OD} - \frac{1}{a} \quad (4)$$

where  $\phi_{OD}$  is the solvent concentration at the ordering transition and  $a$  is an empirical constant that depends on the dynamics of the particular polymer–solvent pair. The PS-*b*-PDMS 5.2–10 and PS-*b*-PDMS 12–22 copolymers should have similar solution dynamics as a function of solvent concentration, so the constant “ $a$ ” in eq 4 should not differ greatly between them. However  $\phi_{OD}$  should decrease with decreasing degree of polymerization,  $N$ , where  $\phi_{OD}$  scales with the degree of segregation,  $\chi N$ .<sup>72</sup> This will make  $\phi_{sc}$  smaller in the lower molecular weight polymer and make perpendicular ordering less favorable as there is a minimum  $\phi_s$  that can be obtained depending on the evaporation rate of the solvent in the drying film. This indicates that there may be a lower molecular weight limit where it is practical to perpendicularly orient PDMS-*b*-PS cylinders regardless of the specific mechanism of ordering. This is of critical concern if high density, small domain size nanostructures are desired. One possible route around this limit is to change the chemistry of the non-PDMS block to increase the  $\chi$  parameter and the overall degree of segregation of the system.

## CONCLUSIONS

The as-spun, thin-film surface morphology of a series of PDMS-rich PS-*b*-PDMS copolymers has been investigated as a function of the casting solvent. PDMS-rich surfaces were obtained regardless of the casting solvent. This is due to the surface activity of the PDMS block, which segregates to the solution–air interface during casting and drives a parallel orientation of the ordered morphology. The surface morphology was found to depend strongly on the solubility parameter of the solvent and SFM images consistent with parallel cylinder, perforated lamellar and lamellar surface layers were observed with increasing solvent solubility parameter. This is attributed to the selective swelling of the individual blocks which even occurs under slightly selective, good solvent conditions. This nontypical behavior is a function of both the low surface

tension of PDMS and the large  $\chi$ . This result has implications for the use of these materials for patterning surfaces. While this offers a route to vary the surface morphology of the film, these results also indicate there may be a lower molecular weight limit at which technologically desirable perpendicular morphologies are practically attainable through spin-coating PS-*b*-PDMS copolymers. While the variation in the surface morphology of as-spun films is not likely useful for applications where long-range order is required since additional processing will be carried out erasing this sample history they could be useful for other applications. This method does provide a facile method to different topographical templates using a single copolymer. This could be useful for probing the effect of nanostructure on adhesive and wetting properties and tissue engineering. Cell adhesion is known to be effected by the substrate stiffness and effects can be correlated to nanostructure features.<sup>74,75</sup> PDMS films have been used as substrates for these experiments.<sup>76</sup> The combination of the surface activity and solvent selectivity effects in these films would provide an interesting nanostructure for these types of experiments where a uniform PDMS surface is created, but the stiffness at the nanoscale could vary due to the arrangement of the underlying surface morphology.

## ASSOCIATED CONTENT

### Supporting Information

Water contact angles, H<sub>2</sub>O contact angles, a TEM micrograph, and SFM phase images. This material is available free of charge via the Internet at <http://pubs.acs.org>

## AUTHOR INFORMATION

### Corresponding Author

\*E-mail: [kac58@uakron.edu](mailto:kac58@uakron.edu). Telephone: 330-972-8368.

### Present Address

<sup>§</sup>DuPont, 974 Centre Road, Chestnut Run Bldg 722/1038A, Wilmington, DE 19805

### Notes

The authors declare no competing financial interest.

## ACKNOWLEDGMENTS

Acknowledgment is made to the University of Akron (M.L.W.) and National Science Foundation under Grant DMR-0906898 for support of this research. K.A.C. acknowledges helpful discussions with Prof. Gila Stein (University of Houston).

## REFERENCES

- (1) Hamley, I. *The Physics of Block Copolymers*, 1st ed.; Oxford University Press: Oxford, U.K., and New York, 1998.
- (2) Harrison, C.; Park, M.; Chaikin, P. M.; Register, R. A.; Adamson, D. H. *J. Vac. Sci. Technol., B* **1998**, *16* (2), 544–552.
- (3) Park, C.; Yoon, J.; Thomas, E. L. *Polymer* **2003**, *44* (22), 6725–6760.
- (4) Segalman, R. A. *Mater. Sci. Eng.* **2005**, *R48* (6), 191–226.
- (5) Park, M.; Harrison, C.; Chaikin, P. M.; Register, R. A.; Adamson, D. H. *Science* **1997**, *276* (5317), 1401–1404.
- (6) Russell, T. P.; Thurn-Albrecht, T.; Tuominen, M.; Huang, E.; Hawker, C. J. *Polymer Science and Industrial Research in the Fast-Changing Age. Macromol. Symp.* **2000**, *159*, 77–88.
- (7) Li, M.; Douki, K.; Goto, K.; Li, X.; Coenjarts, C.; Smilgies, D. M.; Ober, C. K. *Chem. Mater.* **2004**, *16* (20), 3800–3808.
- (8) Li, L.; Yokoyama, H. *Angew. Chem., Int. Ed.* **2006**, *45* (38), 6338–6341.
- (9) Jung Yeon, S.; Ross, C. A. *Nano Lett* **2007**, *7* (7), 2046–50.

- (10) Bitá, I.; Yang, J. K. W.; Jung, Y. S.; Ross, C. A.; Thomas, E. L.; Berggren, K. K. *Science (Washington, DC)* **2008**, 321 (5891), 939–943.
- (11) Jung, Y. S.; Jung, W.; Ross, C. A. *Nano Lett.* **2008**, 8 (9), 2975–2981.
- (12) Jung, Y. S.; Ross, C. A. *Adv. Mater.* **2009**, 21 (24), 2540–2545.
- (13) Chao, C.-C.; Wang, T.-C.; Ho, R.-M.; Georgopoulos, P.; Avgeropoulos, A.; Thomas, E. L. *ACS Nano* **2010**, 4 (4), 2088–2094.
- (14) Jung, Y. S.; Chang, J. B.; Verploegen, E.; Berggren, K. K.; Ross, C. A. *Nano Lett.* **2010**, 10 (3), 1000–1005.
- (15) Rodwogin, M. D.; Spanjers, C. S.; Leighton, C.; Hillmyer, M. A. *ACS Nano* **2010**, 4 (2), 725–732.
- (16) Ross, C. A.; Jung, Y. S.; Chuang, V. P.; Ilievski, F.; Yang, J. K. W.; Bitá, I.; Thomas, E. L.; Smith, H. I.; Berggren, K. K.; Vancso, G. J.; Cheng, J. Y. *J. Vac. Sci. Technol., B: Microelectron. Nanometer Struct.—Process., Meas., Phenom.* **2008**, 26 (6), 2489–2494.
- (17) Li, M.; Ober, C. K. *Mater. Today* **2006**, 9 (9), 30–39.
- (18) Albert, J. N. L.; Epps, T. H., III. *Mater. Today* **2010**, 13 (6), 24–33.
- (19) Lin, Z.; Kim, D. H.; Wu, X.; Boosahda, L.; Stone, D.; LaRose, L.; Russell, T. P. *Adv. Mater.* **2002**, 14 (19), 1373–1376.
- (20) Temple, K.; Kulbaba, K.; Power-Billard, K. N.; Mannes, I.; Leach, K. A.; Xu, T.; Russell, T. P.; Hawker, C. J. *Adv. Mater. (Weinheim, Ger.)* **2003**, 15 (4), 297–300.
- (21) Kim, S. H.; Misner, M. J.; Xu, T.; Kimura, M.; Russell, T. P. *Adv. Mater.* **2004**, 16 (3), 226–231.
- (22) Horvat, A.; Lyakhova, K. S.; Sevink, G. J. A.; Zvelindovsky, A. V.; Magerle, R. *J. Chem. Phys.* **2004**, 120 (2), 1117–1126.
- (23) Knoll, A.; Magerle, R.; Krausch, G. *J. Chem. Phys.* **2004**, 120 (2), 1105–1116.
- (24) Harant, A. W.; Bowman, C. N. *J. Vac. Sci. Technol., B: Microelectron. Nanometer Struct.—Process., Meas., Phenom.* **2005**, 23 (4), 1615–1621.
- (25) Kim, G.; Libera, M. *Macromolecules* **1998**, 31 (8), 2569–2577.
- (26) Kim, S. H.; Misner, M. J.; Russell, T. P. *Adv. Mater.* **2008**, 20 (24), 4851–4856.
- (27) Turturro, A.; Gattiglia, E.; Vacca, P.; Viola, G. T. *Polymer* **1995**, 36 (21), 3987–96.
- (28) Hansen, C. M., *Hansen solubility parameters: a user's handbook*; CRC Press: Boca Raton, FL, 2000.
- (29) Brandrup, J.; Immergut, E. H., *Polymer Handbook*, 4th ed.; John Wiley & Sons: New York, 1998.
- (30) Phillip, W. A.; Hillmyer, M. A.; Cussler, E. L. *Macromolecules* **2010**, 43 (18), 7763–7770.
- (31) Wadley, M. L.; Cavicchi, K. A. *J. Appl. Polym. Sci.* **2010**, 115 (2), 635–640.
- (32) Mark, J. E., *Polymer data handbook*; Oxford University Press: New York and Oxford, U.K., 1999.
- (33) Forster, S.; Timmann, A.; Konrad, M.; Schellbach, C.; Meyer, A.; Funari, S. S.; Mulvaney, P.; Knott, R. *J. Phys. Chem. B* **2005**, 109 (4), 1347–60.
- (34) Chu, J. H.; Rangarajan, P.; Adams, J. L.; Register, R. A. *Polymer* **1995**, 36 (8), 1569–75.
- (35) Matsen, M. W.; Bates, F. S. *J. Polym. Sci., Part B: Polym. Phys.* **1997**, 35 (6), 945–952.
- (36) Kikkawa, Y.; Kurokawa, K.; Kimura, R.; Takahashi, M.; Kanesato, M.; Abe, H. *Polym. Degrad. Stab.* **2010**, 95 (8), 1414–1420.
- (37) Wang, Q.; Yan, Q.; Nealey, P. F.; De Pablo, J. J. *Macromolecules* **2000**, 33 (12), 4512–4525.
- (38) Huinink, H. P.; Brokken-Zijp, J. C. M.; van Dijk, M. A.; Sevink, G. J. A. *J. Chem. Phys.* **2000**, 112 (5), 2452–2462.
- (39) Yang, Y.; Qiu, F.; Zhang, H.; Yang, Y. *Polymer* **2006**, 47 (6), 2205–2216.
- (40) Park, I.; Park, S.; Park, H.-W.; Chang, T.; Yang, H.; Ryu, C. Y. *Macromolecules* **2006**, 39 (1), 315–318.
- (41) Gong, Y.; Huang, H.; Hu, Z.; Chen, Y.; Chen, D.; Wang, Z.; He, T. *Macromolecules* **2006**, 39 (9), 3369–3376.
- (42) Tsarkova, L.; Knoll, A.; Krausch, G.; Magerle, R. *Macromolecules* **2006**, 39 (10), 3608–3615.
- (43) Jung, J.; Park, H.-W.; Lee, S.; Lee, H.; Chang, T.; Matsunaga, K.; Jinnai, H. *ACS Nano* **2010**, 4 (6), 3109–3116.
- (44) Knoll, A.; Horvat, A.; Lyakhova, K. S.; Krausch, G.; Sevink, G. J. A.; Zvelindovsky, A. V.; Magerle, R. *Phys. Rev. Lett.* **2002**, 89 (3), 035501/1–035501/4.
- (45) Matsen, M. W.; Bates, F. S. *Macromolecules* **1996**, 29 (23), 7641–7644.
- (46) Hamley, I. W.; Koppi, K. A.; Rosedale, J. H.; Bates, F. S.; Almdal, K.; Mortensen, K. *Macromolecules* **1993**, 26 (22), 5959–70.
- (47) Tsuji, H.; Satoh, H.; Ikeda, S.; Gotoh, Y.; Ishikawa, J. *Nucl. Instrum. Methods Phys. Res., Sect. B* **1998**, 141 (1–4), 197–201.
- (48) Bhattacharya, S.; Datta, A.; Berg, J. M.; Gangopadhyay, S. *J. Microelectromech. Syst.* **2005**, 14 (3), 590–597.
- (49) Haubert, K.; Drier, T.; Beebe, D. *Lab Chip* **2006**, 6 (12), 1548–1549.
- (50) Wu, N.; Zheng, A.; Huang, Y.; Liu, H. *J. Appl. Polym. Sci.* **2007**, 104 (2), 1010–1018.
- (51) Wu, N.; Zheng, A.; Huang, Y.; Yao, W.; Liu, H. *J. Appl. Polym. Sci. B* **2006**, 44 (13), 1835–1845.
- (52) Guan, C.-M.; Luo, Z.-H.; Tang, P.-P. *J. Appl. Polym. Sci.* **2010**, 116 (6), 3283–3290.
- (53) Clark, D. T.; Peeling, J.; O'Malley, J. M. *J. Polym. Sci., Part A Polym. Chem.* **1976**, 14 (3), 543–51.
- (54) Chan, C.-M., *Polymer Surface modification and characterization*; Hanser Gardner Publications: Munich, Germany, 1994.
- (55) Owen, M. J.; Kendrick, T. C. *Macromolecules* **1970**, 3 (4), 458–61.
- (56) Kent, M. S.; Lee, L. T.; Factor, B. J.; Rondelez, F.; Smith, G. S. *J. Chem. Phys.* **1995**, 103 (6), 2320–42.
- (57) Kent, M. S. *Macromol. Rapid Commun.* **2000**, 21 (6), 243–270.
- (58) Leger, L.; Silberzan, P. *J. Phys., Cond. Matt.* **1990**, 2, SA421–SA425.
- (59) Jasper, J. J. *J. Phys. Chem. Ref. Data* **1972**, 1 (4), 841–1009.
- (60) Smallwood, I. M. *Handbook of Organic Solvent Properties*; John Wiley & Sons: New York, 1996.
- (61) Luciani, A.; Champagne, M. F.; Utracki, L. A. *Polym. Networks Blends* **1996**, 6 (2), 51–62.
- (62) Kim, S.; Briber, R. M.; Karim, A.; Jones, R. L.; Kim, H.-C. *Macromolecules* **2007**, 40 (12), 4102–4105.
- (63) Flory, P. J. *Principles of polymer chemistry*; Cornell University Press: Ithaca, NY, 1953.
- (64) Huang, C.-I.; Lodge, T. P. *Macromolecules* **1998**, 31 (11), 3556–3565.
- (65) Bang, J.; Kim, B. J.; Stein, G. E.; Russell, T. P.; Li, X.; Wang, J.; Kramer, E. J.; Hawker, C. J. *Macromolecules* **2007**, 40, 7019–7025.
- (66) Paik, M. Y.; Bosworth, J. K.; Smilges, D.-M.; Schwartz, E. L.; Andre, X.; Ober, C. K. *Macromolecules* **2010**, 43 (9), 4253–4260.
- (67) Lodge, T. P.; Hamersky, M. W.; Hanley, K. J.; Huang, C.-I. *Macromolecules* **1997**, 30 (20), 6139–6149.
- (68) Zhang, Q.; Tsui, O. K. C.; Du, B.; Zhang, F.; Tang, T.; He, T. *Macromolecules* **2000**, 33 (26), 9561–9567.
- (69) Huang, H.; Zhang, F.; Hu, Z.; Du, B.; He, T.; Lee, F. K.; Wang, Y.; Tsui, O. K. C. *Macromolecules* **2003**, 36 (11), 4084–4092.
- (70) Huang, H.; Hu, Z.; Chen, Y.; Zhang, F.; Gong, Y.; He, T.; Wu, C. *Macromolecules* **2004**, 37 (17), 6523–6530.
- (71) Gong, Y.; Hu, Z.; Chen, Y.; Huang, H.; He, T. *Langmuir* **2005**, 21 (25), 11870–11877.
- (72) Hanley, K. J.; Lodge, T. P. *J. Polym. Sci., Part B: Polym. Phys.* **1998**, 36 (17), 3101–3113.
- (73) Park, S.; Wang, J.-Y.; Kim, B.; Chen, W.; Russell, T. P. *Macromolecules* **2007**, 40 (25), 9059–9063.
- (74) Heydarkhan-Hagvall, S.; Choi, C.-H.; Dunn, J.; Heydarkhan, S.; Schenke-Layland, K.; MacLellan, W. R.; Beygui, R. E. *Cell Commun. Adhes.* **2008**, 14 (5), 181–194.
- (75) Discher, D. E.; Janmey, P.; Wang, Y.-I. *Science* **2005**, 310 (5751), 1139–1143.
- (76) Kidambi, S.; Udpa, N.; Schroeder, S. A.; Findlan, R.; Lee, I.; Chan, C. *Tissue Eng.* **2007**, 13 (8), 2105–2117.